# Preonset time sequence of auroral substorms: Coordinated observations by all-sky imagers, satellites, and radars

Y. Nishimura,[1,2] L. R. Lyons,[1] S. Zou,[3] X. Xing,[1] V. Angelopoulos,[4] S. B. Mende,[5] J. W. Bonnell,[5] D. Larson,[5] U. Auster,[6] T. Hori,[2] N. Nishitani,[2] K. Hosokawa,[7] G. Sofko,[8] M. Nicolls,[9] and C. Heinselman[9]

Received 17 June 2010; revised 23 August 2010; accepted 3 September 2010; published 24 November 2010.

[1] Using two conjunction events of the Time History of Events and Macroscale Interactions during Substorms (THEMIS) imagers and spacecraft as well as the Super Dual Auroral Radar Network (SuperDARN) and Poker Flat Incoherent Scatter Radars, we show that longitudinally narrow flow bursts in the nightside polar cap can precede poleward boundary intensifications (PBIs) that are followed by equatorward moving north-south (N-S) arcs, including those leading to substorm onset instability within the near-Earth plasma sheet. The association between the ionospheric flows and PBIs indicates that enhanced flows on open field lines may contribute to parallel potential drop increase, triggering of magnetotail reconnection, and to the earthward flows leading to N-S arcs and to substorm onset. We also investigated differences between N-S arc sequences that do and do not lead to substorm expansion onset. We found that the two types of N-S arcs have similar characteristics, indicating that their corresponding plasma sheet flow properties could also be similar. There is, however, one difference between the sequences of N-S arc evolution. Each N-S arc leads to small intensification of the growth phase arc, and when the onset-related N-S arc reaches the equatorward portion of the auroral oval, the preexisting growth phase arc is much brighter than at the times of non-onset-related N-S arcs. Assuming that the growth phase arc is related to pressure gradients at the inner edge of the plasma sheet, this difference indicates that the near-Earth plasma pressure distribution at the time of plasma sheet fast flows is crucial in substorm triggering. These observations suggest that substorm onset instability is possible only when the preexisting inner plasma sheet pressure is sufficiently large.

**Citation:** Nishimura, Y., et al. (2010), Preonset time sequence of auroral substorms: Coordinated observations by all-sky imagers, satellites, and radars, *J. Geophys. Res.*, *115*, A00I08, doi:10.1029/2010JA015832.

## 1. Introduction

[2] There has been a long-lasting debate on the preonset sequence of substorms. Recently, evidence for plasma flow enhancements in the magnetotail prior to onset has been presented, suggesting magnetic reconnection in the midtail plasma sheet preceding substorm onset in the near-Earth plasma sheet [*Kepko et al.*, 2004; *Angelopoulos et al.*, 2008]. On the other hand, auroral onset occurring near the equatorward boundary of the auroral oval supports an idea that near-Earth instability precedes magnetic reconnection and earthward plasma flows [*Lui and Burrows*, 1978; *Donovan et al.*, 2008; *Akasofu et al.*, 2010].

[3] Recently, *Nishimura et al.* [2010] proposed a potential resolution to this problem based on observations from the Time History of Events and Macroscale Interactions during Substorms (THEMIS) all-sky imager (ASI) array, which provides high spatial and temporal resolution auroral images with broad latitudinal and longitudinal coverage [*Mende et al.*, 2008]. They found that the preonset auroral sequence is initiated by a poleward boundary intensification (PBI), which is followed by an approximately north-south (N-S) oriented

[1]Department of Atmospheric and Ocean Sciences, University of California, Los Angeles, California, USA.
[2]Solar-Terrestrial Environment Laboratory, Nagoya University, Nagoya, Aichi, Japan.
[3]Department of Atmospheric, Oceanic and Space Sciences, University of Michigan, Ann Arbor, Michigan, USA.
[4]Institute of Geophysics and Planetary Physics, University of California, Los Angeles, California, USA.
[5]Space Sciences Laboratory, University of California, Berkeley, California, USA.
[6]Institut für Geophysik und Extraterrestrische Physik, Technischen Universität Braunschweig, Braunschweig, Germany.
[7]Department of Information and Communication Engineering, University of Electro-Communications, Chofu-shi, Tokyo, Japan.
[8]Department of Physics and Engineering, University of Saskatchewan, Saskatoon, Saskatchewan, Canada.
[9]Center for Geospace Studies, SRI International, Menlo Park, California, USA.


0148-0227/10/2010JA015832

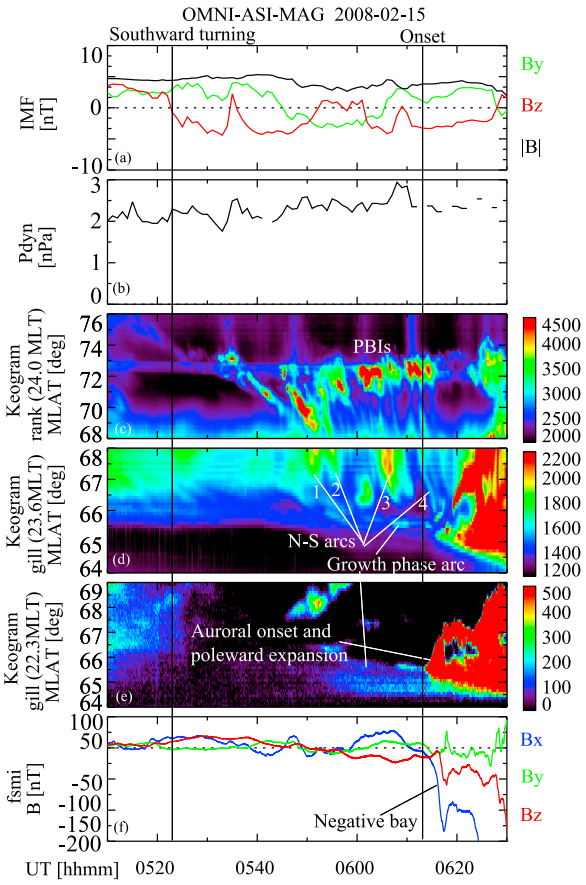


**Figure 1.** OMNI solar wind data, auroral keograms at Rankin Inlet (RANK) and Gilliam (GILL), and ground magnetometer data at Fort Smith (FSMI) at 0510–0630 UT on 15 February 2008. The first interplanetary magnetic field (IMF) southward turning and substorm onset times are marked by the vertical lines. The keograms were obtained at three different longitudes. The magnetic local times (MLTs) given are at the time of the onset. Four N-S arcs marked in Figure 1d and investigated in Figures 2 and 5 are numbered as 1–4.

arc (also called auroral streamer) moving equatorward toward the onset latitude and leading to onset instability in the near-Earth plasma sheet. Because of the linkage of fast magnetotail flows to PBIs and to N-S auroras, this sequence gives strong support to an idea that onset instability develops following enhanced plasma flows from the open-closed boundary toward the near-Earth plasma sheet. The high occurrence rate of PBIs and N-S arcs preceding substorm onset indicates that equatorward motion of preonset aurora, as previously found for a case by *Oguti* [1973] and by *Kepko et al.* [2009], may be common and possibly related to PBIs at higher latitudes, which suggests preceding magnetic reconnection near the nightside open-closed field line boundary. In the present study, we expand upon several fundamental aspects of the preonset substorm sequence found by *Nishimura et al.* [2010].

[4] *Xing et al.* [2010] investigated space-ground conjunctions using the THEMIS spacecraft and ASIs when preonset N-S arcs were detected near the footprints of the spacecraft. They identified earthward enhanced plasma flows having reduced pressure in the magnetotail simultaneously with N-S arcs near the footprints of the spacecraft. This is consistent with new plasma injection toward the near-Earth plasma sheet, where the plasma presumably has lower entropy than the surround plasma [*Wolf et al.*, 2009]. However, while N-S arcs have been generally associated with fast earthward flows, these are often not associated with a substorm onset [*Nakamura et al.*, 1993, 2001; *Sergeev et al.*, 2000; *Henderson et al.*, 2002]. Therefore, the difference between N-S arc sequences that do and do not lead to substorm onset within the near-Earth plasma sheet is an outstanding question for understanding the connection between plasma sheet enhanced flows and substorm onset. Furthermore, flow observation associated with preonset aurora have not yet been reported from simultaneously magnetospheric and ionospheric observations, and such coordinated observations are required in order to understand plasma conditions in the near-Earth plasma sheet when earthward fast flows associated with N-S arcs reach that region.

[5] Another question is the initiation of preonset PBIs, which mark the beginning of the preonset auroral sequence. *Angelopoulos et al.* [2008, 2009] showed enhanced plasma inflows at the outer boundary of the plasma sheet toward the center of the plasma sheet prior to onset using the THEMIS spacecraft. *Lyons et al.* [2010b] found that such inflows are common along the entire length of the open-closed field lines when there are PBIs that are followed by N-S arcs and substorm onset, and J. Liu et al. (Superposed epoch analysis of magnetotail flux transport during substorms observed by THEMIS, submitted to *Journal of Geophysical Research*, 2010) showed that the sequence is statistically significant using a few dozen substorms in the GEM substorm database. Observations of ionospheric plasma flows have a capability to determine evolution of such flows since ionospheric flow bursts are known to be associated with PBIs and following equatorward motion [*de la Beaujardiere et al.*, 1994]. *Lyons et al.* [2010a] found evidence from ionospheric radar observations that these flows commonly traverse the open-closed field line boundary, suggesting that the flow enhancements initiating the preonset sequence are not localized around the open-closed boundary but are related to polar cap convection. These results and inferences would indicate that enhanced convection on open polar cap field lines plays an essential role in triggering the reconnection that is associated with the initiation of the preonset auroral sequence. Such triggering is envisioned in some computer models of reconnection onset [*Birn et al.*, 2005; *Pritchett*, 2005]. Investigations of spatial and temporal variations of plasma convection in the nightside polar cap associated with PBIs are thus essential for understanding the initiation of the preonset time sequence.

[6] The present study focuses on three aspects that are critical for understanding the preonset sequence: (1) what does trigger PBIs that begin the preonset sequence?, (2) what is the difference between N-S arc sequences that do and do not lead to substorm onset?, and (3) does an enhanced flow channel exist both in the ionosphere and magnetosphere associated with a preonset N-S arc? We present two conjunction events of ASIs, radars and spacecraft during substorms. Radar observations from the Super Dual Auroral Radar Network (SuperDARN) [*Greenwald et al.*, 1995] and Poker Flat Incoherent Scatter Radar (PFISR) [*Nicolls et al.*, 2007], have an advantage of detecting two-dimensional

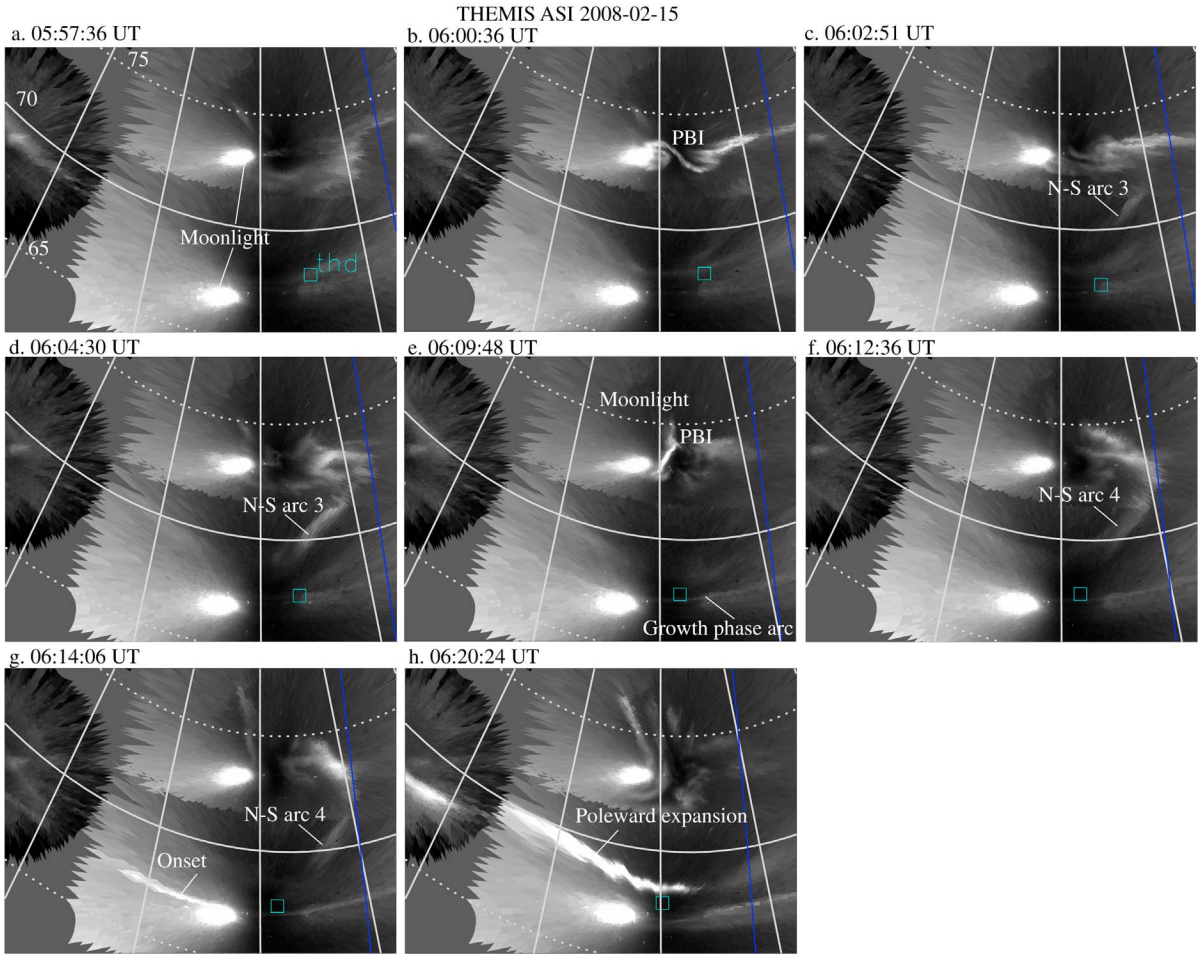


**Figure 2.** Selected snapshots of THEMIS ASI data during an auroral onset on 15 February 2008. ASIs used are RANK (65.13° magnetic latitude (MLAT) and 253.47° magnetic longitude (MLON)), GILL (67.24° MLAT and 266.14° MLON), and Fort Simpson (FSIM) (67.30° MLAT and 293.85° MLON). White lines are isocontours of magnetic latitude (every 5°) and longitude (every 15°). The blue lines and light blue squares are the magnetic midnight meridian and THEMIS-D footprint using T96. The onset occurred at 0613:21 UT. The entire sequence is shown in Animation 1.

distributions of plasma flows which may be associated with PBIs and N-S arcs. Corresponding plasma sheet flows are investigated using the THEMIS spacecraft [*Sibeck and Angelopoulos*, 2008]. Our analysis for one of the events shows a one to one correspondence between PBIs and preceding polar cap flow bursts, suggesting that the polar cap flow bursts contribute to the initiation of reconnection and PBIs. For both events, we find that the growth phase arc, which lies at the lowest-latitude portion of the auroral oval, is much brighter when the onset-related N-S arc reaches the equatorward portion of the oval, while no significant difference in N-S arc properties is identified. This suggests that the near-Earth plasma condition at the times of plasma sheet fast flows is crucial in triggering of substorm onset instability.

## 2. THEMIS-SuperDARN Conjunction (15 February 2008 Substorm)

### 2.1. Auroral Sequence

[7] Figure 1 shows OMNI solar wind data, auroral keograms from the ASIs at Rankin Inlet (RANK) and GILL, and ground magnetometer data at Fort Smith (FSMI) during a substorm with onset at 0613 UT on 15 February 2008. The interplanetary magnetic field (IMF) turned southward at ~0523 UT after a ~1.5 h northward IMF period, and the auroral oval was in a quiet state at this time as can be seen in Figures 1c to 1e. Auroral activity at the poleward boundary of the auroral oval around magnetic midnight increased after 0531 UT, and multiple PBIs can be identified in Figure 1c. Here, PBIs refer to auroral intensifications near the poleward boundary above 3000 counts/sec in the RANK imager, and the poleward boundary is the poleward edge of the polewardmost auroral emissions, which is located at magnetic latitude $\Lambda$ ~73° in Figure 1c as is typical [*Blanchard et al.*, 1995]. N-S arcs originated from PBIs moved equatorward as can be seen in the drifting auroral forms in Figures 1c and 1d (Figure 1c shows emissions above $\Lambda$ = 68°, and Figure 1d shows emissions slightly to the west from the lower-latitude imager at GILL from $\Lambda$ = 64–68°). N-S arcs investigated in detail in this study are numbered as 1–4.

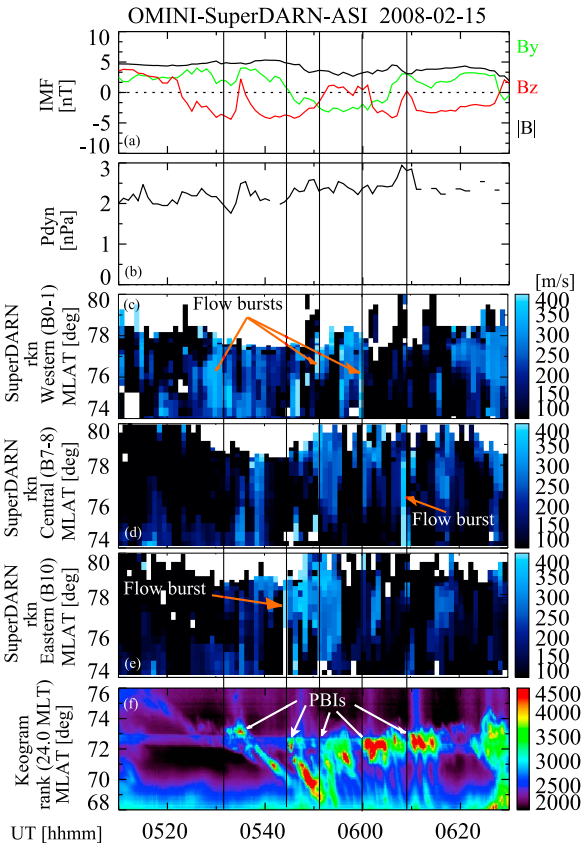


**Figure 3.** Comparison between the SuperDARN l-o-s velocity and the auroral keogram at Rankin Inlet. The latitudinal profiles of the flow were obtained from beams 0 and 1 averaging (westward looking), 7 and 8 averaging (northward looking), and 10 (eastward looking). Positive is directed toward the radar. Vertical lines mark PBI initiation times. Flow bursts preceding or simultaneous with PBIs are marked by red arrows.

[8] As seen from the emissions in Figures 1d and 1e (1.3 magnetic local time (MLT) apart), the auroral oval near the equatorward boundary was quiet with a gradual intensification of the diffuse, lowest-latitude aurora (labeled "growth phase arc") until the substorm onset time (second vertical line). The substorm onset is identified as substantial auroral intensification near the equatorward boundary followed by poleward expansion (Figure 1e) and the development of a negative magnetic bay (Figure 1f). The absence of auroral disturbance near the equatorward boundary and only small magnetic field perturbations prior to the onset indicate that this was an isolated substorm.

[9] Figure 2 shows a sequence of images from three ASIs during the substorm (see Animation 1 for the entire image sequence).[1] The light blue square is the THEMIS-D footprint using the Tsyganenko 96 magnetic field model [*Tsyganenko and Stern*, 1996]. The auroral oval was quiet in the first image except for the weak intensification near the poleward boundary in the RANK imager field of view (FOV) and the faint growth phase arc near the equatorward boundary in Fort Simpson (FSIM). A PBI initiated at ~0558 UT and further intensified at ~0600 UT near the center of the RANK imager FOV and extended azimuthally (Figure 2b). An N-S arc originating from the PBI moved equatorward and westward (Figures 2c and 2d, N-S arc 3 in Figure 1d), and disappeared by 0610 UT. The N-S arc was not followed by a substorm onset but instead the auroral equatorward boundary remained quiet. It should be noted, however, that a thin arc along the poleward edge of the preexisting diffuse-like growth phase arc started to be more discernible after the N-S arc reached the equatorward portion of the auroral oval. This arc can be seen as a latitudinally narrow emission in Figures 1e, 2e, and 2f, where the narrowness would be characteristics of discrete aurora arcs, which are associated with upward field-aligned currents and downward electron energized by field-aligned electric fields.

[10] The next PBI occurred at 0609 UT as a longitudinally narrow auroral form (Figure 2e) and led to an N-S arc moving equatorward and westward (Figure 2f, N-S arc 4 in Figure 1d). Note that the evolution of the N-S arc 4 is quite similar to that of the N-S arc 3. In contrast to the N-S arc 3 sequence, the substorm onset followed the N-S arc 4 just to the west of the N-S arc meridian at 0613:21 UT, as can be recognized in Animation 1 and the later image in Figure 1g. Note that a latitudinal gap can be seen between the N-S arc 4 and the newly formed thin growth phase arc just prior to the onset. This gap was also identified in the first event of *Nishimura et al.* [2010] and is interpreted as the flow channel bringing plasma from the open-closed boundary associated with upward field-aligned currents to the right of the flow direction (see section 2.2 for the spatial relation between the flow channel and aurora).

### 2.2. SuperDARN and ASI Observations of Polar Cap Flow Bursts and PBIs

[11] Figure 3 shows latitudinal profiles of the line-of-sight (l-o-s) velocity from the SuperDARN radar at RANK, as well as the solar wind data and the RANK auroral keogram from Figure 1. The radar looks poleward and detects radar echoes at latitudes from just poleward of the auroral poleward boundary to $\Lambda = 80^{\circ}$. The vertical lines show PBI initiation times. The latitudinal profiles of the flow in Figures 3c to 3e were obtained from radar beams 0 and 1 averaging (westward looking), 7 and 8 averaging (northward looking), and 10 (eastward looking). These can be identified as polar cap echoes, based on the absence of auroral emission above ~73° magnetic latitude (MLAT) in Figure 3f. Note that these echoes are mainly *E* region backscatters and thus the flow magnitude may be underestimated and limited below the ion acoustic speed (~400 m/s) [*Haldoupis*, 1989; Koustov *et al.*, 2005]. However, this does not influence on our results because we do not discuss the exact flow magnitude but focus on relative flow changes. Only flows directed toward the radar (i.e., from the polar cap toward the polar cap boundary) are shown, since there only a few small flows directed away from the radar.

[12] A number of flow bursts directed toward the radar can be identified as transient blue strips. Their typical duration is less than a few minutes, and they are localized in longitude. They extend from above $\Lambda = 78^{\circ}$ to near the equatorward boundary of the radar FOV at 74°, indicating that these are longitudinally narrow equatorward flow channels in

[1] Animations are available in the HTML.

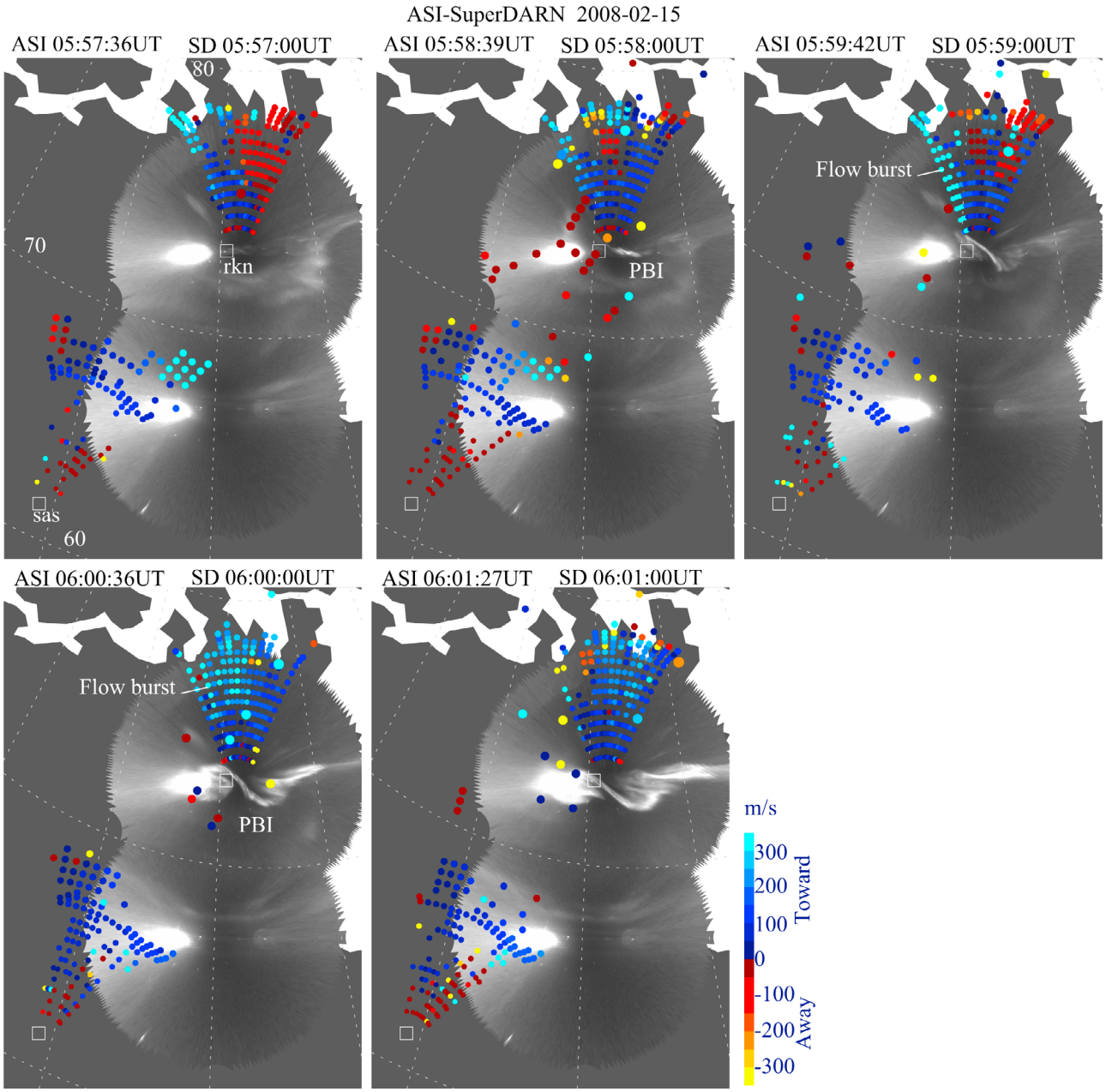


**Figure 4a.** Spatial distribution of the SuperDARN l-o-s velocity (RANK and Saskatoon) overlaid onto the ASI data (RANK and GILL) between 0557 and 0602 UT.

the nightside polar cap. As indicated by the vertical lines and red arrows, the flow bursts tend to occur prior to or simultaneously with the PBIs to within the 1 min time resolution of the SuperDARN observations. For example, the 0609 UT PBI (the last vertical line in Figure 3f) was preceded by the flow burst at 0608 UT in Figure 3d. Flow bursts which are not marked by red arrows in Figure 3 are also related to further auroral intensifications near the poleward boundary.

[13] Two-dimensional l-o-s flow distributions and auroral observations are shown in Figure 4 to display the relation between the polar cap flows and PBIs in more detail. Figure 4a includes the PBI shown in Figure 2b. The measured flow was initially weak and probably directed to the east as can be inferred from the positive and negative l-o-s velocity at the western and eastern beams, respectively. A small PBI occurred at 0558 UT as seen in Figure 4a (top middle). The flow in RANK near the poleward boundary of the oval did not increase substantially until this time, which might be because the flow channel was located further to the west of the FOV. A flow burst was first detected clearly in the western beams of Figure 4a (top right). It can be identified as southeastward flows because of the positive velocity confined to the western beams, and the flows in the western beams Figure 4a (top left and top middle) indicate that it may have rapidly propagated equatorward from higher latitudes. The flow burst occurred ~1 min earlier than

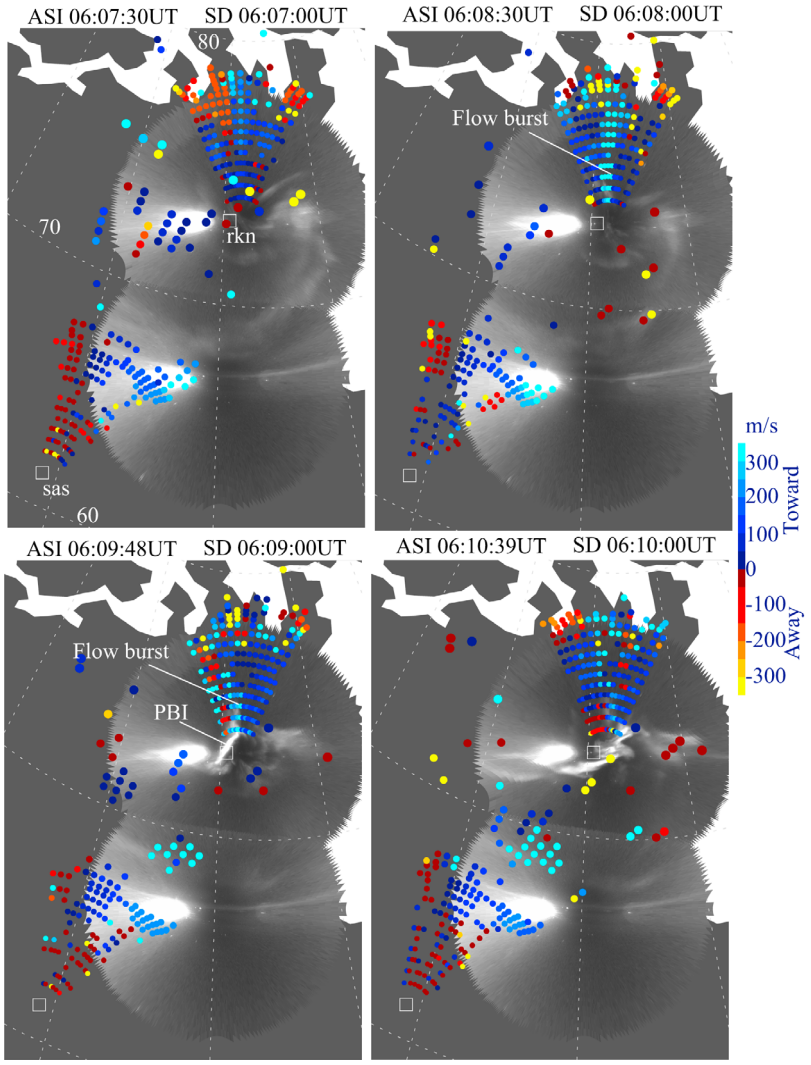


**Figure 4b.** Same as Figure 4a but for between 0607 and 0611 UT.

the further intensification of the PBI (Figure 4a, bottom left) and then the enhanced flow and PBI both extended in longitude (Figure 4a, bottom left and bottom right).

[14] Figure 4b is for the PBI shown in Figure 2e. The flow magnitude was small for a few minutes and mainly directed westward until 0608 UT. The flow burst occurred in the central meridian of the RANK radar at 0608 UT (Figure 4b, top right), clearly showing a longitudinally narrow (~0.2 MLT width) region of enhanced equatorward flows in the polar cap extending down to the poleward boundary of the auroral oval. The PBI occurred ~1 min later at the same longitude or slightly to the west of the enhanced flow channel (Figure 4b, bottom left). Furthermore, the MLT widths of the flow burst and PBI are about the same. The flow burst can still be seen in the equatorward portion of the radar FOV as weaker flows in Figure 4b (bottom right).

[15] The spatial correspondence between the PBIs and preceding flow bursts suggests that enhanced flows in the polar cap contribute to PBI triggering, including those PBIs which mark the beginning of the auroral sequence leading to substorm onset. It is further noted that the flow bursts tend to be located slightly to the east of or the same meridian as the PBIs. This is consistent with the geometry of the flow channel in the magnetosphere, where upward and downward field-aligned currents are formed to the west and east of the flow channel [*Birn et al.*, 2004; *Sergeev et al.*, 2004], while the flows were measured on open field lines. The spatial and temporal association of the flow bursts and PBIs shown in Figures 3 and 4 suggests that the flow bursts in the entire length of the separatrix strengthen the parallel potential drop at the low-altitude magnetosphere. The reconnection signature cannot be seen at the times of PBI initiation because of the Alfvén wave propagation time delay of approximately a few minutes, but the equatorward-drifting N-S arcs following to the PBIs, which are described in section 2.3, imply the reconnection triggering associated with the flow bursts.

### 2.3. ASI Observations of N-S Arcs and Onset

[16] We shift our focus to the multiple N-S arcs originating from the PBIs reaching the equatorward portion of

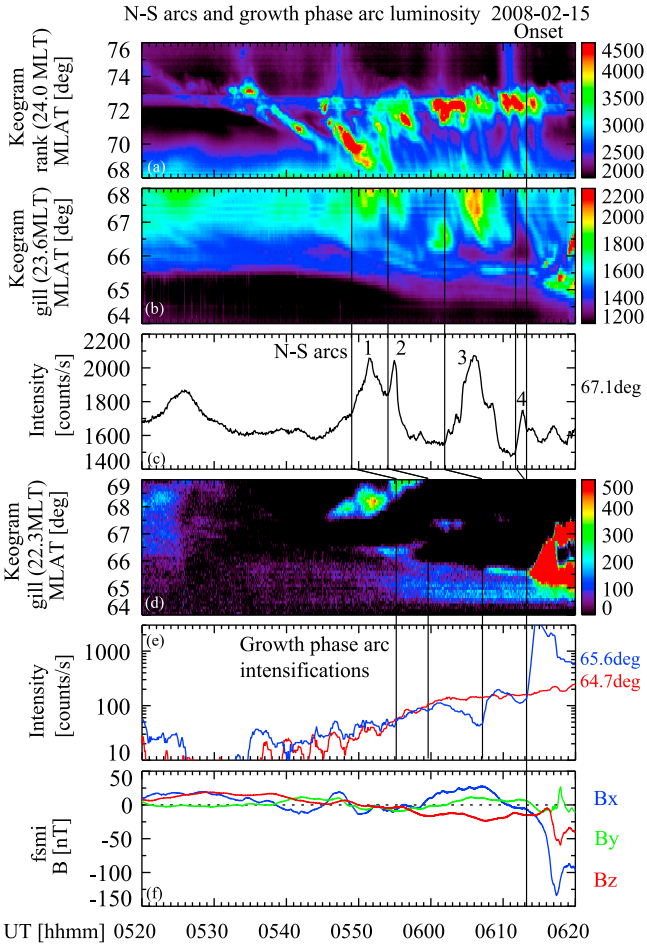


**Figure 5.** Line plots of the auroral intensity at 67.1° MLAT from Figure 5b (Figure 5c) and 64.7° (red) and 65.6° (blue) MLAT from Figure 5d (Figure 5e). The auroral keograms and magnetograms are the same as in Figure 1. The vertical lines only in Figures 5b and 5c mark the arrival of the N-S arcs. The vertical lines only in Figures 5d and 5e indicates growth phase arc intensifications. The last vertical line marks the substorm onset time. Numbers 1–4 in Figure 5c refer the four N-S arcs as in Figure 1.

the auroral oval. Figures 5c and 5e give the auroral intensity at 67.1° MLAT from Figure 5b and at 64.7° (red) and 65.6° (blue) MLAT from Figure 5d, in addition to the keograms and magnetogram shown in Figure 1, respectively. These curves in Figures 5c and 5e represent intensity variations of the N-S arcs and growth phase arc, respectively. The four N-S arcs 1–4 can be seen as rapid increases in intensity followed by equatorward motion. We have not found an identifiable difference in the intensity, propagation speed or spatial size between the N-S arcs 1–3 and N-S arc 4 that may account for why N-S arc 4 lead to a substorm and the others did not. Rather, the N-S arc 4 was weaker in intensity than the other arcs at the meridian shown in Figures 5b and 5c.

[17] Figures 5d and e show time evolutions of the intensity of the growth phase arc. While the intensity increased monotonically at lower latitudes (red line in Figure 5e), intensity increases at the poleward portion of the preexisting diffuse-like growth phase arc (blue line in Figure 5e), where the thin arc is observed, are seen a few minutes after each of the N-S arcs reaches near the growth arc to the east of this meridian. This is consistent with an idea that these intensity variations result from plasma pressure changes in the near-Earth plasma sheet resulting from newly supplied plasma, which is associated with the N-S arcs and then drifts azimuthally from the N-S arc meridian. After 0607 UT, following the third N-S arc, these intensity variations became discernible as a separate arc, which is seen as a thin arc in Figure 2e. This arc developed into the onset arc soon after the N-S arc 4 reached the equatorward portion of the auroral oval, when the growth phase arc was much brighter than that at the times of the previous N-S arcs.

[18] The difference in the growth phase arc intensity at the times of the approaching N-S arc suggests that the near-Earth plasma condition was different when the arc-associated enhanced plasma flows intruded to the plasma sheet from outer *L*-shells of the plasma sheet. While each of the plasma sheet flow enhancements seems to have similar properties, the enhanced plasma pressure, which presumably leads to the brighter growth phase arc, may thus play an essential role in whether or not there is a substorm onset after enhanced flows reach the near-Earth plasma sheet. While all the enhanced flow into this region caused some increase in auroral intensity near the onset latitude, the flow that led to onset instability occurred during the time when the auroral observations suggest that the inner plasma sheet pressure was the highest.

### 2.4. THEMIS Spacecraft Observations

[19] Figure 6 shows THEMIS-D spacecraft observations in the near-Earth plasma sheet near the meridian of the N-S arcs. The dominance of Bx in Figure 6a and the thermal pressure in Figure 6c indicates that the spacecraft was located in the plasma sheet close to but slightly to the south of its center. A notable feature is enhancements of the azimuthal flow moment (Vy) in Figure 6d prior to the onset as marked by the vertical lines. These flow enhancements may not be attributed to the E × B drift but to pressure gradient [*Baumjohann and Treumann*, 1996], since the (E × B)y in Figure 6e is much smaller, except for intermittent E × B flow enhancements.

[20] Compared with Figure 5, the azimuthal flow enhancements (except the 0539 UT flows indicated by the dashed line) are found to occur between the times of the N-S arcs and the thin growth phase arc intensifications. If the azimuthal flow is mainly associated with the pressure gradient, the westward flow enhancements can be interpreted as pressure gradient enhancements in the z direction (earthward when mapped along field lines to the equatorial plane) that could lead to enhanced field-aligned currents and thus to the growth phase arc intensifications. (This should not be considered as the effect of decreasing magnetic field because the magnetic field was increasing or almost constant when the azimuthal flow speed increased. Effects of the earthward pressure gradient would be small because the magnetic field is dominated by Bx.) The spacecraft observation supports our suggestion that plasma transport from the midtail to the near-Earth plasma sheet associated with the N-S arcs leads to pressure gradient increases and thus to an enhanced region 2 current system

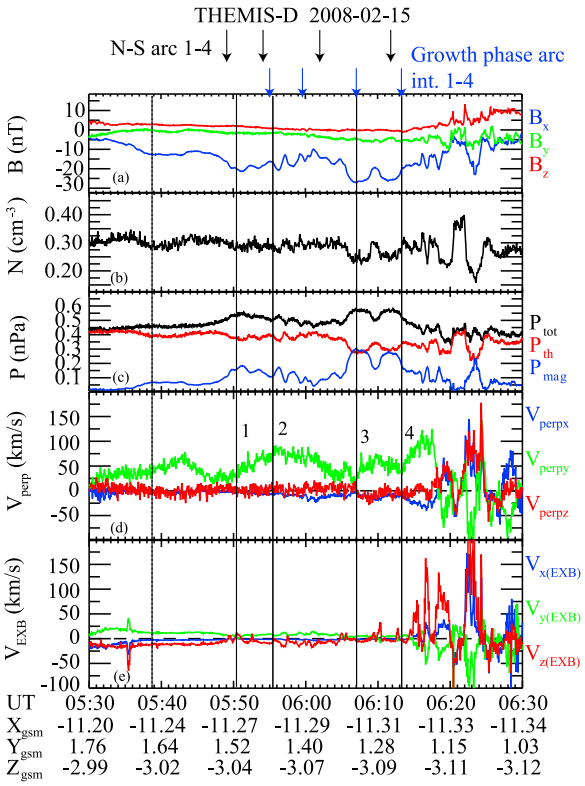


**Figure 6.** THEMIS-D spacecraft data between 0530 and 0630 UT on 15 February 2008. Geocentric solar magnetospheric magnetic field, density, pressure, velocity moment, and E × B drift speed are shown. The E × B drift speed was calculated only from the spin plane electric fields. The vertical lines mark Vy flow enhancements. The last vertical line also corresponds to the substorm onset time. The flow enhancements marked by numbers 1–4 in Figure 6d occurred soon after the times of the N-S arcs 1–4. The timings of the N-S arcs and growth phase arc intensifications in Figure 5 are shown by black and blue arrows on the top of the figure. The third component of the electric field (Ez) was obtained from the E dot B = 0 assumption.

with the intensifications of the narrow arc on the poleward portion of the preexisting diffuse-like growth phase arc at the footprint of the upward region 2 field-aligned currents that lie poleward of the downward region 2 current in the Harang reversal region [*Gkioulidou et al.*, 2009]. This leads to the speculation that the substorm was triggered when the enhanced flow led to a change in the pressure gradient that was larger than for the earlier N-S arcs.

## 3. THEMIS-PFISR Conjunction (15 February 2009 Substorm)

[21] The presence of an earthward flow channel conjugate to a preonset N-S arc has been suggested by ground-based radar and spacecraft observations separately [*Sergeev et al.*, 2000; *Lyons et al.*, 2010b; X. Xing et al., submitted manuscript, 2010]. In this section, we present a conjunction event where the PFISR and THEMIS spacecraft footprint were located close to an N-S arc, which supports the above suggestion by showing such enhanced flows simultaneously in both the magnetosphere and ionosphere.

### 3.1. Auroral Sequence

[22] Figure 7 shows OMNI solar wind data, auroral keograms from Inuvik (INUV) and Fort Yukon (FYKN), and ground magnetometer data at Bettles (BETT) during a substorm which occurred at 1128 UT on 15 February 2009. The IMF turned southward at ~1042 UT (not shown) and stayed southward until the onset time. PBIs occurred at 1111 and 1120 UT as can be seen in Figure 7c. An N-S arc originating from the second PBI moved equatorward (Figures 7c and d). The substorm onset is identified as the auroral intensification near the equatorward boundary (Figure 7e) associated with the negative magnetic bay (Figure 7f). Note that the substorm was preceded by small intensifications seen in Animation 2. starting at ~1113:30 and 1118:30 UT (which reached the meridian of Figure 7e at ~1121 UT) but these disturbances ceased by the time of the onset. Similar to the previous event, the diffuse-like growth phase arc just before the onset started to gradually become brighter for several minutes prior to the onset near

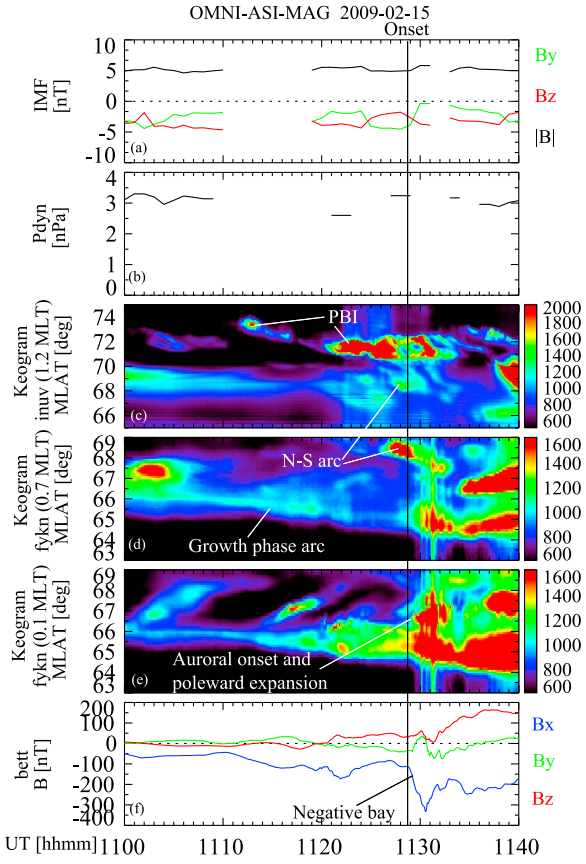


**Figure 7.** OMNI solar wind data, auroral keograms at Inuvik (INUV) and Fort Yukon (FYKN), and ground magnetometer data at Bettles (BETT) at 1030–1140 UT on 15 February 2009. The substorm onset time is marked by the vertical line. The keograms were obtained at three different longitudes. The MLTs given are at the time of the onset.

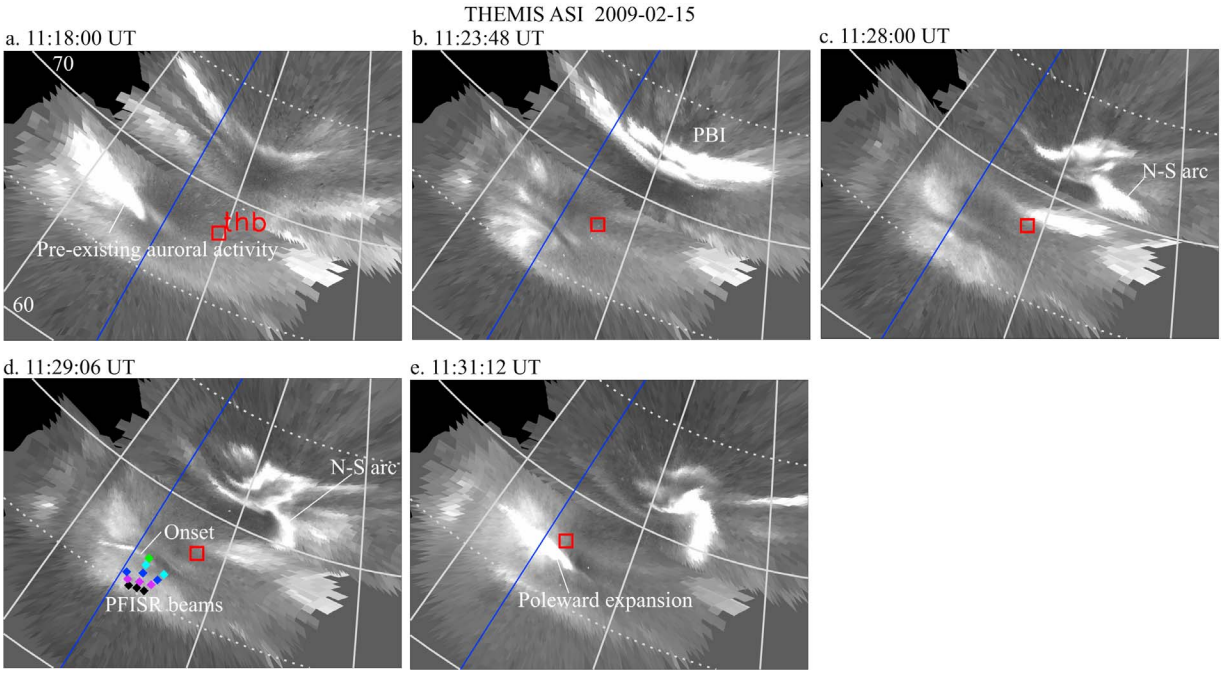


**Figure 8.** Selected snapshots of THEMIS ASI data during an auroral onset on 15 February 2008. ASIs used are INUV (71.23° MLAT and 275.09° MLON) and FYKN (67.24° MLAT and 266.14° MLON). White lines are isocontours of magnetic latitude (every 5°) and longitude (every 15°). The blue lines and red squares are the magnetic midnight meridian and THEMIS-B footprint using T96. The onset occurred at 1128:51 UT. Colored dots in Figure 8d mark the locations of PFISR beam segments shown in Figure 9. The entire sequence is shown in Animation 2.

the onset meridian, forming a thin arc, as shown in Figure 7e. This is an indication that the plasma pressure in the near-Earth plasma sheet became higher than at earlier times.

[23] Figure 8 shows the sequence of images from two ASIs during the substorm (see Animation 2 for the entire image sequence). The red square shows the THEMIS-B footprint using T96. The PBI occurred at ~73° MLAT as can be seen in Figure 8b. The N-S arc with clockwise rotation moved equatorward and westward (Figures 8c and 8d), and the substorm auroral onset occurred at ~67° MLAT just to the west of the N-S arc meridian. Further intensification and poleward expansion can be seen in Figure 8e. The flow channel would be located so that the N-S arc would be to the right of the flow direction. Thus the higher-latitude data points (blue, light blue, and green in Figure 8d) of the PFISR beams are expected to observe the enhanced plasma flow located south of the low-latitude, westward extension of the arc and supplying plasma toward the onset location.

### 3.2. PFISR Observations

[24] Figure 9 shows latitudinal profiles of the PFISR l-o-s velocity from (a) eastward, (b) northward, and (c) westward looking beams. Positive is directed away from the radar. A negative flow enhancement started at ~1116 UT at the eastward and northward looking beams and then extended to the westward looking beam. The negative flow in all directions can be interpreted as flows with an equatorward component under enhanced convection and may be a flow enhancement preceding the auroral disturbance starting at ~1118 UT, though we do not focus on this feature. A further negative flow enhancement occurred after the PBI prior to the substorm onset, as indicated by the second vertical line ~4 min after the PBI. This flow enhancement was concurrent with the equatorward moving N-S arc which was located along approximately the same meridian. Thus, the enhanced flow may correspond to equatorward plasma flows, which are expected to exist to the east of the N-S arc in a converging electric field geometry. The southwestward plasma flow prior to the onset indicates a plasma supply leading to the substorm onset, consistent with what was shown by *Lyons et al.* [2010a] and the schematic picture shown by *Nishimura et al.* [2010, Figure 11]. The flow increase then reached the westward looking beam just before or at the onset time, which was measured as an increase in plasma flow indicating westward flows, although the l-o-s flow was still negative due to the coexistence of the equatorward flow as seen in Figure 9b.

### 3.3. THEMIS Spacecraft Observations

[25] As shown in Figure 8d, the THEMIS-B spacecraft footprint was located close to the N-S arc and a little to the north and east of the PFISR FOV, allowing the possibility of detecting the flow channel associated with the arc in the magnetosphere as well as in the ionosphere. Figure 10 shows the spacecraft data in the same format as Figure 6. The plasma pressure was higher than the magnetic pressure for most of the time and the large negative Bx prior to the onset indicate that the spacecraft was located close to but slightly to the south of the center of the plasma sheet.

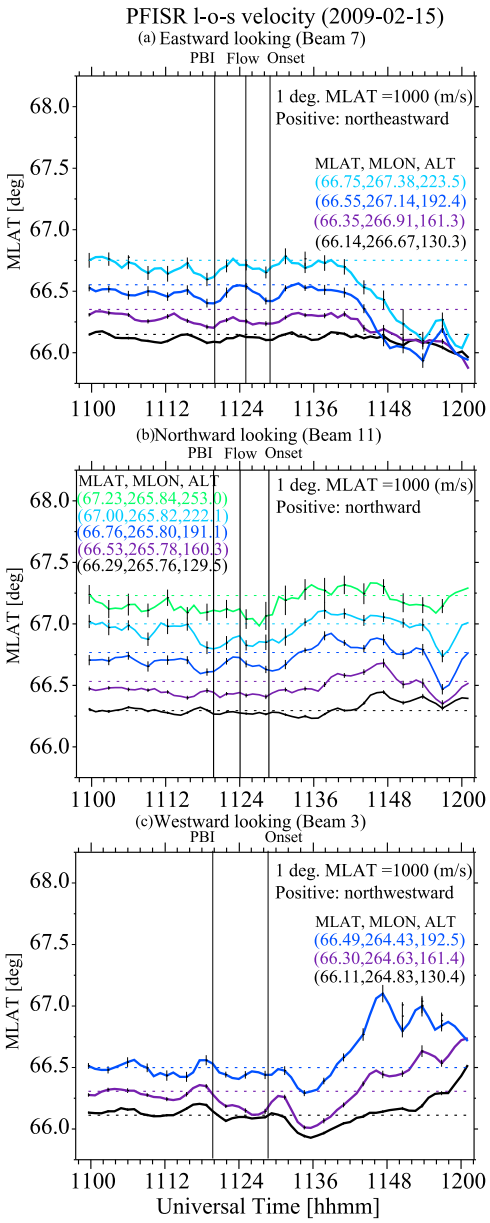


**Figure 9.** PFISR l-o-s velocity from (a) eastward looking (beam 7), (b) northward looking (beam 11), and (c) westward looking (beam 3) beams. The vertical axis shows MLAT of base lines (dashed lines), and the deviations (solid lines) show the l-o-s flow velocity. Positive is defined as flows away flow the radar. MLAT, MLON, and altitude (ALT) of each line are given. The vertical lines mark the PBI, flow enhancement in Figure 9a, and onset times. The beam locations are also shown in Figure 8d.

[26] As marked by the second vertical line, an azimuthal flow enhancement followed by an equatorward flow (Vz > 0) was observed after the PBI and ~5 min prior to the onset. The azimuthal flow was measured simultaneously with the flow enhancement detected by PFISR (Figure 9a) within the time resolution of PFISR (1 min). The following equatorward flow corresponds to an earthward flow when mapped along field lines to the equator, indicating an equatorward flow in the ionosphere. These flow directions are also consistent with the equatorward and westward N-S arc motion. In spite of the intermittent availability of the E × B flow, roughly a half of the enhancements of Vy and Vz at ~1126 and 1127 UT is contributed by the electric drift, suggesting that the spacecraft measured enhanced plasma flows in the plasma sheet corresponding to the flow channel in the ionosphere adjacent to the N-S arc. These coordinated observations by ASIs, PFISR and spacecraft lead us to conclude that the enhanced plasma flow, possibly associated with magnetic reconnection as inferred from the PBI, forms both in the magnetosphere and ionosphere and brings new plasma population toward the near-Earth plasma sheet leading to substorm onset. More ASI-spacecraft conjunction events of preonset N-S arcs were investigated in detail by *Xing et al.* [2010], indicating that the preonset plasma flow channel forming in the magnetosphere-ionosphere coupled system is a common feature of substorms.

## 4. Conclusion

[27] We have presented two conjunctions of ASIs, radars and spacecraft during substorms to investigate the relation between the preonset auroral sequence and enhanced plasma flows in the magnetosphere-ionosphere coupled system.

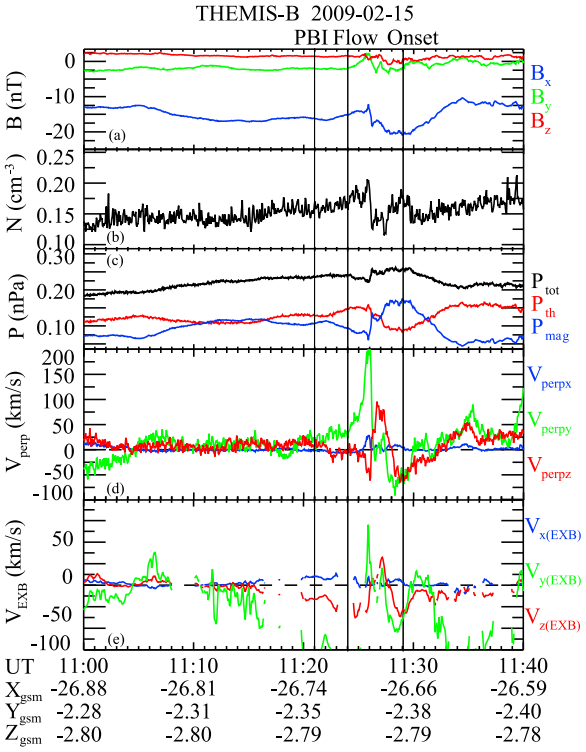


**Figure 10.** THEMIS-B spacecraft data between 1100 and 1140 UT on 15 February 2009. The format is the same as Figure 6. The vertical lines mark the PBI, Vy flow enhancement and onset times. The third component of the electric field (Ez) was obtained from the E dot B = 0 assumption. The data gap in Figure 10e arises from unavailability of Ez due to small angles of the magnetic field and spin plane (<1°).

Both of the events show the preonset auroral sequence, which starts from a PBI that is followed by an N-S arc moving toward the onset location and then by onset near the equatorward boundary of the auroral oval, consistent with the findings of *Nishimura et al.* [2010].

[28] By taking an advantage of the SuperDARN two-dimensional observations coordinated with auroral imaging, we have shown for the first event that the observed PBIs were preceded by polar cap flow bursts and that the flow bursts are found to have narrow longitudinal widths (~0.2 MLT) and short durations (a few minutes). The longitudinal extent of PBIs has a correspondence with those of the flow bursts. These results lead us to suggest that enhanced flows in the polar cap may contribute to parallel potential drop increase at the low-altitude magnetosphere. The reconnection in the magnetotail is also inferred to be triggered when the flow bursts reach the plasma sheet, based on the following equatorward moving N-S arcs. Thus, the flow bursts on open field lines initiate the auroral time sequence leading to substorm onset.

[29] For the first event, multiple equatorward moving N-S arcs originated from the PBIs and moved toward the growth phase arc. However, only one of these led to the onset, and we did not find any significant difference in N-S arc features. On the other hand, all of the N-S arcs were found to be related to intensification of a narrow arc along the poleward boundary of the preexisting diffuse-like growth phase arc. For both of the events, the growth phase arc at the time of the last N-S arc before the onset was much brighter than at preceding times. This difference leads us to suggest that the near-Earth plasma condition was not sufficient for substorm onset instability at the times of the preceding N-S arcs, and in particular that the plasma pressure in the near-Earth plasma sheet was not sufficiently large until the time period of the onset-related N-S arc.

[30] The existence of the preonset flow channel was suggested in the first event and by *Lyons et al.* [2010b] and *Xing et al.* [2010], however, there has not been simultaneous flow observations in the magnetosphere and ionosphere. PFISR observations for the second event showed the enhanced plasma flow associated with the equatorward moving preonset N-S arc, and this plasma flow was observed simultaneously by the THEMIS spacecraft in approximately the conjugate region within the plasma sheet. The simultaneous occurrence of the enhanced flow suggests that an enhanced flow channel extends from the magnetosphere to the ionosphere and brings a new plasma population toward the near-Earth plasma sheet leading to substorm onset.

[31] Noting that the upward field-aligned currents and downward electron energization associated with discrete auroral arcs can be driven by plasma sheet pressure gradients, the above simultaneous observations, lead us to speculate that the growth phase arc intensifications and the substorm onset aurora resulted from the enhanced flows prior to onset leading to pressure gradient changes within the near-Earth plasma sheet, and that the onset instability was possible only when the preexisting inner plasma sheet pressure was sufficiently large. Both this speculation and our suggestion that enhanced flows within the polar cap initiate PBIs and the auroral time sequence leading to substorm onset are based only on the two events discussed here and the relevant preceding results referred to in the text. We believe that these possibilities warrant further in depth studies.

[32] **Acknowledgments.** This work was supported by National Science Foundation grants ATM-0646233 and ATM-0639312, NASA grant NNX07AF66, NASA contract NAS5–02099, DLR contract 50 OC 0302 for the THEMIS/FGM instruments, and JSPS Research Fellowships for Young Scientists. Deployment and data retrieval of the THEMIS ASIs was partly supported by CSA contract 9F007–046101. We thank J. McFadden and C. W. Carlson for providing the ESA data.

[33] Robert Lysak thanks the reviewers for their assistance in evaluating this paper.

## References

Akasofu, S.-I., A. Lui, and C.-I. Meng (2010), Importance of auroral features in the search for substorm onset processes, *J. Geophys. Res.*, *115*, A08218, doi:10.1029/2009JA014960.

Angelopoulos, V., et al. (2008), Tail reconnection triggering substorm onset, *Science*, *321*, 931, doi:10.1126/science.1160495.

Angelopoulos, V., et al. (2009), Response to comment on "Tail reconnection triggering substorm onset," *Science*, *324*, 1391, doi:10.1126/science.1168045.

Baumjohann, W., and R. Treumann (1996), *Basic Space Plasma Physics*, Imperial College, London.

Birn, J., J. Raeder, Y. Wang, R. Wolf, and M. Hesse (2004), On the propagation of bubbles in the geomagnetic tail, *Ann. Geophys.*, *22*, 1773, doi:10.5194/angeo-22-1773-2004.

Birn, J., et al. (2005), Forced magnetic reconnection, *Geophys. Res. Lett.*, *32*, L06105, doi:10.1029/2004GL022058.

Blanchard, G. T., L. R. Lyons, J. C. Samson, and F. J. Rich (1995), Locating the polar cap boundary from observations of 6300 Å auroral emission, *J. Geophys. Res.*, *100*, 7855, doi:10.1029/94JA02631.

de la Beaujardiere, O., L. R. Lyons, J. M. Ruohoniemi, E. Friis-Christensen, C. Danielsen, F. J. Rich, and P. T. Newell (1994), Quiet-time intensifications along the poleward auroral boundary near midnight, *J. Geophys. Res.*, *99*, 287–298, doi:10.1029/93JA01947.

Donovan, E., et al. (2008), Simultaneous THEMIS in situ and auroral observations of a small substorm, *Geophys. Res. Lett.*, *35*, L17S18, doi:10.1029/2008GL033794.

Gkioulidou, M., C.-P. Wang, L. R. Lyons, and R. A. Wolf (2009), Formation of the Harang reversal and its dependence on plasma sheet conditions: Rice convection model simulations, *J. Geophys. Res.*, *114*, A07204, doi:10.1029/2008JA013955.

Greenwald, R. A., et al. (1995), DARN/SuperDARN: A global view of the dynamics of high-latitude convection, *Space Sci. Rev.*, *71*, 761, doi:10.1007/BF00751350.

Haldoupis, C. (1989), A review on radio studies of auroral *E* region ionospheric irregularities, *Ann. Geophys.*, *7*, 239.

Henderson, M. G., L. Kepko, H. E. Spence, M. Connors, J. B. Sigwarth, L. A. Frank, H. J. Singer, and K. Yumoto (2002), The evolution of north-south aligned auroral forms into auroral torch structures: The generation of omega bands and Ps6 pulsations via flow bursts, paper presented at the Sixth International Conference on Substorms, Univ. of Wash., Seattle, Wash.

Kepko, L., M. G. Kivelson, R. L. McPherron, and H. E. Spence (2004), Relative timing of substorm onset phenomena, *J. Geophys. Res.*, *109*, A04203, doi:10.1029/2003JA010285.

Kepko, L., E. Spanswick, V. Angelopoulos, E. Donovan, J. McFadden, K. Glassmeier, J. Raeder, and H. J. Singer (2009), Equatorward moving auroral signatures of a flow burst observed prior to auroral onset, *Geophys. Res. Lett.*, *36*, L24104, doi:10.1029/2009GL041476.

Koustov, A. V., D. W. Danskin, R. A. Makarevitch, and J. D. Gorin (2005), On the relationship between the velocity of *E* region HF echoes and $E \times B$ plasma drift, *Ann. Geophys.*, *23*, 371, doi:10.5194/angeo-23-371-2005.

Lui, A. T. Y., and J. R. Burrows (1978), On the location of auroral arcs near substorm onsets, *J. Geophys. Res.*, *83*, 3342, doi:10.1029/JA083iA07p03342.

Lyons, L. R., Y. Nishimura, Y. Shi, S. Zou, H.-J. Kim, V. Angelopoulos, C. Heinselman, M. J. Nicolls, and K.-H. Fornacon (2010a), Substorm triggering by new plasma intrusion: Incoherent-scatter radar observations, *J. Geophys. Res.*, *115*, A07223, doi:10.1029/2009JA015168.

Lyons, L. R., Y. Nishimura, X. Xing, V. Angelopoulos, S. Zou, D. Larson, J. McFadden, A. Runov, S. Mende, and K.-H. Fornacon (2010b), Enhanced transport across entire length of plasma sheet boundary field lines leading to substorm onset, *J. Geophys. Res.*, doi:10.1029/2010JA015831, in press.

Mende, S. B., S. E. Harris, H. U. Frey, V. Angelopoulos, C. T. Russell, E. Donovan, B. Jackel, M. Greffen, and L. M. Peticolas (2008), The THEMIS array of ground-based observatories for the study of auroral substorms, *Space Sci. Rev.*, *141*, 357, doi:10.1007/s11214-008-9380-x.

Nakamura, R., T. Oguti, T. Yamamoto, and S. Kokubun (1993), Equatorward and poleward expansion of the auroras during auroral substorms, *J. Geophys. Res.*, *98*, 5743, doi:10.1029/92JA02230.

Nakamura, R., W. Baumjohann, R. Schödel, M. Brittnacher, V. A. Sergeev, M. Kubyshkina, T. Mukai, and K. Liou (2001), Earthward flow bursts, auroral streamers, and small expansions, *J. Geophys. Res.*, *106*, 10,791, doi:10.1029/2000JA000306.

Nicolls, M. J., C. J. Heinselman, E. A. Hope, S. Ranjan, M. C. Kelley, and J. D. Kelly (2007), Imaging of Polar Mesosphere Summer Echoes with the 450 MHz Poker Flat Advanced Modular Incoherent Scatter Radar, *Geophys. Res. Lett.*, *34*, L20102, doi:10.1029/2007GL031476.

Nishimura, Y., L. Lyons, S. Zou, V. Angelopoulos, and S. Mende (2010), Substorm triggering by new plasma intrusion: THEMIS all-sky imager observations, *J. Geophys. Res.*, *115*, A07222, doi:10.1029/2009JA015166.

Oguti, T. (1973), Hydrogen emission and electron aurora at the onset of the auroral breakup, *J. Geophys. Res.*, *78*, 7543, doi:10.1029/JA078i031p07543.

Pritchett, P. L. (2005), Externally driven magnetic reconnection in the presence of a normal magnetic field, *J. Geophys. Res.*, *110*, A05209, doi:10.1029/2004JA010948.

Sergeev, V. A., et al. (2000), Multiple-spacecraft observation of a narrow transient plasma jet in the Earth's plasma sheet, *Geophys. Res. Lett.*, *27*, 851, doi:10.1029/1999GL010729.

Sergeev, V., K. Liou, P. Newell, S. Ohtani, M. Hairston, and F. Rich (2004), Auroral streamers: Characteristics of associated precipitation, convection and field-aligned currents, *Ann. Geophys.*, *22*, 537, doi:10.5194/angeo-22-537-2004.

Sibeck, D. G., and V. Angelopoulos (2008), THEMIS science objectives and mission phases, *Space Sci. Rev.*, *141*, 35, doi:10.1007/s11214-008-9393-5.

Tsyganenko, N. A., and D. P. Stern (1996), Modeling the global magnetic field of the large-scale Birkeland current systems, *J. Geophys. Res.*, *101*, 27,187, doi:10.1029/96JA02735.

Wolf, R. A., Y. Wan, X. Xing, J.-C. Zhang, and S. Sazykin (2009), Entropy and plasma sheet transport, *J. Geophys. Res.*, *114*, A00D05, doi:10.1029/2009JA014044.

Xing, X., L. Lyons, Y. Nishimura, V. Angelopoulos, D. Larson, C. Carlson, J. Bonnell, and U. Auster (2010), Substorm onset by new plasma intrusion: THEMIS spacecraft observations, *J. Geophys. Res.*, *115*, A10246, doi:10.1029/2010JA015528.

V. Angelopoulos, Institute of Geophysics and Planetary Physics, University of California, Los Angeles, 3845 Slichter Hall, Los Angeles, CA 90095, USA.

U. Auster, Institut für Geophysik und Extraterrestrische Physik, Technischen Universität Braunschweig, Mendelssohnstrasse 3, D-38106 Braunschweig, Germany.

J. W. Bonnell, D. Larson, and S. B. Mende, Space Sciences Laboratory, University of California, 7 Gauss Way, Berkeley, CA 94720, USA.

C. Heinselman and M. Nicolls, Center for Geospace Studies, SRI International, 333 Ravenswood Ave., Menlo Park, CA 94025, USA.

K. Hosokawa, Department of Information and Communication Engineering, University of Electro-Communications, 1-5-1 Chofugaoka, Chofu-shi, Tokyo 182-8585, Japan.

L. R. Lyons, Y. Nishimura, and X. Xing, Department of Atmospheric and Oceanic Sciences, University of California, Los Angeles, 405 Hilgard Ave., 7127 Math Sciences Bldg., Los Angeles, CA 90095-1565, USA. (toshi@atmos.ucla.edu)

N. Nishitani and T. Hori, Solar-Terrestrial Environment Laboratory, Nagoya University, Furocho, Chikusa, Nagoya, Aichi 464-8601, Japan.

G. Sofko, Department of Physics and Engineering, University of Saskatchewan, 116 Science Pl., Saskatoon, SK S7N 5E2, Canada.

S. Zou, Department of Atmospheric, Oceanic and Space Sciences, University of Michigan, 2455 Hayward St., Ann Arbor, MI 48109-2143, USA.